Transition of nc-SiC powder surface into grain boundaries during sintering by molecular dynamics simulation and neutron powder diffraction

M. Wojdyr[1,2], I. Szlufarska[1], Y. Mo[1], E. Grzanka[2], S. Stelmakh[2], S. Gierlotka[2], B. Palosz[2]

[1] Department of Materials Science and Engineering, University of Wisconsin-Madison, Madison, Wisconsin 53706-1595, USA

[2] Institute of High Pressure Physics, Polish Academy of Sciences, ul. Sokolowska 29/37, 01-142 Warsaw, Poland

Keywords: powder diffraction, molecular dynamics, silicon carbide, Debye formula

Abstract. We report a structural analysis of experimental nc-SiC ceramics with grain sizes ranging from 7 nm to 11 nm in diameter and computer generated samples of similar grain sizes. Pair Distribution Functions (PDFs) of real and virtual samples sintered under different pressures are compared. The standard size-strain methods are applied to the simulated models and the results are discussed. Presented model is the first step toward atomistic understanding of the processing-structure relations and atomic-level interpretation of diffraction patterns for nanoceramics.

Introduction

Silicon Carbide (SiC) based ceramics have many technological applications, which originate from their remarkable physical and chemical properties, *e.g.* high hardness, high melting temperature, light weight, and chemical stability. It is known that decreasing the grain size of polycrystalline ceramics to the nanometre regime can further improve their mechanical properties [1-3]. For example, recent experiments on nanocrystalline (nc) SiC have demonstrated an increased hardness of this material [4]. Atomistic mechanisms underlying this so-called superhardness of nc-SiC have been revealed in recent computer simulations [5]. Despite of all the promising properties of nc-SiC, a detailed understanding of the processing – structure – property relations in this material is still lacking.

X-ray and neutron diffractions are powerful and commonly used techniques for microstructure characterization; however, analysis of diffraction patterns of nc materials presents additional challenges. Due to an increased surface-to-volume ratio of nanoparticles, grain boundaries (GB) occupy a significant volume-fraction of the material and the coherently

scattering domains become very small. As a result, positions of the diffraction peaks are not consistent with the Bragg law [6] and become dependent on the grain size and shape [7], and specific structure of grain boundaries [8], in addition to the well-established dependence on lattice parameters.

Molecular Dynamics (MD) simulations provide trajectories of all the atoms, giving a direct view of the microstructure. Therefore coupling diffraction techniques with MD simulations opens up new possibilities for structural investigation of nanomaterials [9]. Such studies have been recently done in nc metals. For example, Derlet *et al.* [10] calculated diffraction patterns for MD models of nc-Ni. The values of size and strain obtained with the Williamson-Hall method and the Debye-Waller factors were shown to be in agreement with the values extracted directly from the model. The nc ceramics have an increased volume fraction of disordered grain boundaries as compared to nc metals [11]. This disorder brings in an additional challenge in extracting structural information and comparing simulation and experimental diffraction spectra.

In this paper we report a joint neutron scattering and MD simulation studies of structural correlations (e.g., pair distribution function, PDF) of nc-SiC for varying sintering pressures. We discuss the effect of sintering conditions on the GB formation.

Experimental and MD procedures

Experimental neutron diffraction data reported here were collected for scattering vectors Q of up to 50 $Å^{-1}$ with NPDF instrument at the Los Alamos Neutron Science Center. We examined the structure of nc-SiC powders, with grain sizes in the range between 10 nm and 40 nm, sintered under pressures of up to 8 GPa and at the temperature of 1,900K. Our virtual nc-SiC samples were prepared in MD simulations of sintering. The details of the interatomic potential used in this study can be found in Refs. [11,12]. Equations of motion are integrated using Verlet-velocity algorithm with a time step of 2.2 fs.

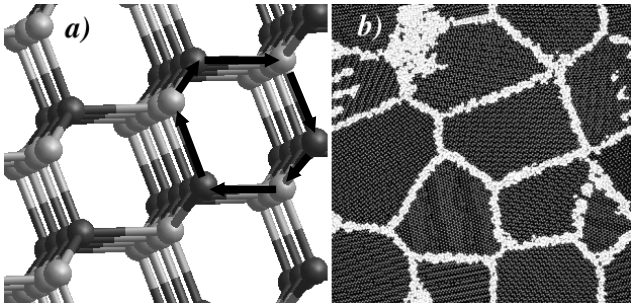

Figure 1. a) Definition of a ring. The shortest closed path (marked by black arrows) includes 3 Si-C pairs and constitutes a 3-fold ring. In a zinc-blende structure, each atom participates in 12 unique 3-fold rings. b) Crystalline atoms (grey) and grain boundaries (white) in MD sample 10.5nm sintered in 7GPa based on the ring analysis criterion.

The initial system has been prepared using Voronoi construction [13], which results in grains shaped as random polyhedra and average dimensions equal to the desired grain size. Each grain has a perfect cubic lattice and a random orientation. We prepared four samples with the

average grain sizes, *d*, equal either 7 nm or 10.5 nm, and each sample was comprised of 32 grains. For each grain size, one sample was sintered at the pressure of 7GPa and one at 12GPa. The sintering temperature for all samples was 1,800K.

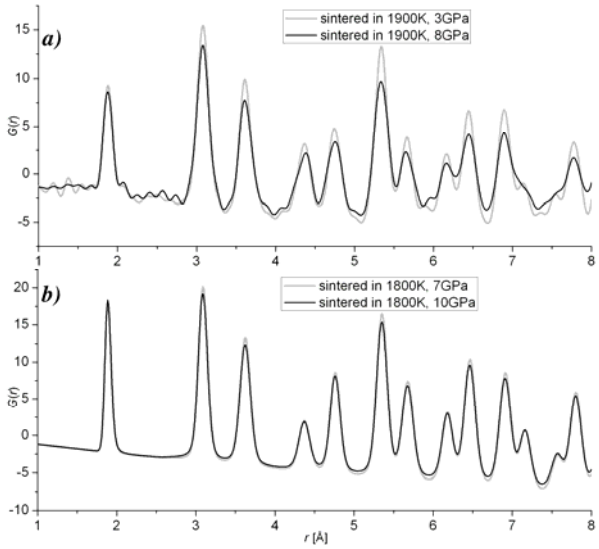

Figure 2. Reduced PDF, G(R), of SiC ceramics: experimental (a) and from MD simulation (b). In both plots the grey line corresponds to lower sintering pressures as compared to the data marked with a black line.

To distinguish GBs from the grains with perfect lattice topology, we employed a ring distribution analysis. Ring analysis has been successfully employed in our earlier studies to identify typological changes in nc-SiC during indentation [12]. A ring is defined as the shortest closed path of alternating Si and C atoms (see figure 1a). In the perfect zinc-blend structure, the shortest ring is 3-fold (the path has 6 atoms), and each atom has 12 distinct 3-fold rings. Based on the ring criterion we identified atoms with a perfect medium-range order (*crystalline atoms)*, and atoms with a distorted medium-range order (*GB atoms)*. In figure 1b, the crystalline and GB atoms are marked as grey and white, respectively.

We calculated the theoretical scattering intensities, based on the Debye formula [14], for interatomic distances of up to 10 nm and 15 nm, for d = 7nm and d = 10.5 nm samples, respectively. Beyond this cut-off distance, we assumed a uniform spatial distribution of atoms. The calculations were done using a publicly available software *Debyer* [15].

Pair Distribution Functions

The PDF analysis has been successfully applied to study structural properties in nc materials [16-19]. A reduced PDF function, $G(r)$, is related to the total scattering structure function $S(Q)$ through the following equation [16]:

$$G(r) = 4\pi r\rho_0(g(r)-1) = \frac{2}{\pi}\int_0^\infty Q[S(Q)-1]\sin(Qr)dQ \cdot \qquad (1)$$

Figure 2a shows $G(r)$ for two experimental samples, both with the average grain size of d = 8nm, which were sintered at a temperature T = 1900K and under pressures of 3GPa and 8 GPa. The $G(r)$ functions for computer-generated samples with d = 7 nm and sintered under pressures 7 GPa and 10 GPa, are shown in figure 2b.
For both experimental and simulated samples larger sintering pressure results in more disordered structures, which is indicated by broader peaks in the $G(r)$ plots. In the model samples, we observed large deviations of local hydrostatic stresses at GBs, which indicates the presence of microstrains. The distinction between GB regions and grains is not strict and therefore the larger microstrain accumulated at GBs can be also viewed as thicker disordered GB.
A closer look at the $G(r)$ and $g(r)$ functions of the MD model shows an asymmetry of peaks, which is not visible in experimental samples most likely due to limitations of the experimental instruments. The asymmetry can be quantified as the difference between the weighted average of the first $g(r)$ peak and the maximum of the peak, which is shown in table 1. We speculate that this phenomenon is related to the difference between the atomic bond elongations in tension and compression at a given temperature. Studies of structural correlations in nc-SiC as a function of temperature are under way [20].
In the data presented in table 1 we also make a distinction between averages calculated for all atoms and for crystalline atoms only. It can be seen that the lattice parameters calculated from diffraction patterns of the samples are in good agreement with the weighted average of $g(r)$ peaks calculated for crystalline atoms.

Table1. Lattice parameter calculated from the first peak in g(r) and from simulated diffraction pattern. Due to asymmetry of g(r) peaks, weighted average (av) of the peak position is different than peak maximum. Crystalline atoms are the ones with a perfect medium-range order.

sample	all atoms		crystalline atoms		diffraction pattern
	av	maximum	av	maximum	
7 nm 7GPa	4.3745	4.3567	4.3707	4.3578	4.3712
7 nm 10GPa	4.3765	4.3578	4.3708	4.3579	4.3713
10.5nm 7GPa	4.3734	4.3578	4.3714	4.3590	4.3718
10.5nm 10GPa	4.3721	4.3578	4.3683	4.3590	4.3695

Size-strain analysis

In experimental data, there are two principal reasons of diffraction line broadening: instrumental factors and physical origins. In the simulated patterns, only the latter is present. The physical broadening is usually divided into size broadening (diffraction-order-independent, caused by finite size of coherent domains) and strain broadening (diffraction-order-dependent, caused by displacements of the atoms from perfect lattice positions).
We employed classical Williamson-Hall (W-H) [21] (see figure 3) and double-Voigt (d-Voigt) [22] methods. Even though, it is widely accepted that the d-Voigt method is based on a better model than W-H and other so-called simplified integral-breadth methods [23], it has

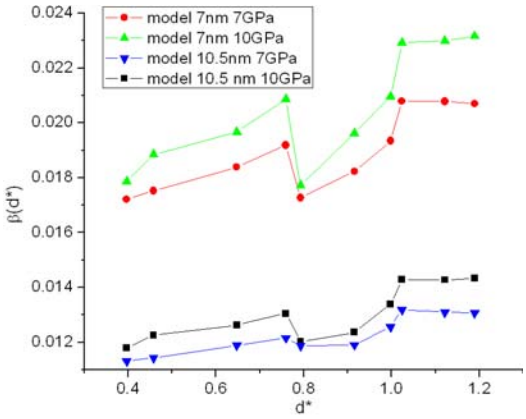

Figure 3. Williamson-Hall plot for data calculated from MD models.

been shown that in the case of nc materials Voigt function leads to an underestimated grain size [24]. Our results (table 2) are consistent this trend and thereby show a need for more sophisticated approaches based on fundamental microstructural parameters.

Table 2. Grain sizes of the MD models. Diffraction patterns calculated from MD models were analysed using standard size-strain methods. $<D>_V$ and $<D>_A$ denote volume- and area-weighted grain size, respectively.

initial grain size	sintering pressure	W-H $<D>_A$[nm]	d-Voigt $<D>_V$ [nm]	% of cryst. atoms
7 nm	7GPa	6.6	6.0	73
7 nm	10GPa	6.7	5.8	70
10.5nm	7GPa	9.7	9.0	81
10.5nm	10GPa	9.5	8.6	76

As shown in table 2, simulation samples that were sintered under higher pressures had a slightly smaller grain size, *i.e*, thicker GBs. It can be explained by the fact, that sintering is driven by surface diffusion [11] and a very high pressure (on the order of 8GPa or more) can possibly suppress this diffusion. As a result, the normally observed high-temperature recrystallization of GBs is inhibited, leading to thicker GBs and smaller crystalline domains [25].

Conclusion

We analysed experimental samples and MD models of nc-SiC ceramics sintered under different pressures. PDF analysis indicates larger disorder in samples sintered under higher pressure. This can be explained by larger microstrains introduced during sintering, and by the inhibited recrystalization due to decreased diffusion at high pressures. The asymmetry in PDF peaks of virtual samples requires further investigation. We speculate that this is caused

by the difference between the atomic bond elongations in tension and compression at a given temperature. We used Williamson-Hall and double-Voigt methods to estimate average grain size of the MD model and compared it with the average size of crystalline regions in the model. Our study is the first step in building an atomic-level understanding of diffraction patterns for nanoceramics and their dependence on processing conditions.

References

1. Zhao, Y.S., Qian, J., Daemen, L., *et al.*, 2004, Appl. Phys. Lett. **84**, 1356.
2. Sumant, A.V., Grierson, D.S., Gerbi, *et al.*, 2005, Adv. Mater. **17**, 1039.
3. Wang, X., Padture, N.P., Tanaka, H., *et al.*, 2005, Acta Mater. **53,** 271.
4. Liao, F., Girshick, S.L., Mook, W.M., *et al.*, 2005, Appl. Phys. Lett.. **86**, 171913.
5. Szlufarska I., Nakano, A., Vashishta, P., 2005, Science **309**, 911.
6. Kaszkur Z., 2000, J. Appl. Cryst.. **33**, 1262.
7. Zanchet, D., Hall, B.D. & Ugarte, D., 2000, in *Characterization of Nanophase Materials*, edited by Z.L. Wang (J. Wiley-VCH, Weinheim, Germany), pp. 13–36.
8. Palosz, B., Grzanka, E., Pantea, *et al.*, 2005, J. Appl. Phys. **97**, 064316.
9. Gilbert, B., Zhang, H.Z., Huang, *et al.*, 2004, J. Chem. Phys. **120**, 11785.
10. Derlet P.M., V. Petegem, S., V. Swygenhoven, H, 2005, Phys. Rev. B **71**, 024114.
11. Chatterjee, A., Kalia, R. K., Nakano, *et al.*, 2000, Appl. Phys. Lett. **77**, 1132.
12. Szlufarska, I., Kalia R.K., Nakano A., *et al.*, 2005, Phys. Rev. B **71**, 174113.
13. Okabe, A., Boots, B., Sugihara, K., *et al.*, 2000, Spatial Tessellations (John Wiley and Sons, New York).
14. Debye, P., 1915, Ann. Phys. **46**, 809.
15. http://www.unipress.waw.pl/debyer
16. Egami, T., Billinge, S., 2003, *Underneath the Bragg Peaks: Structural Analysis of Complex Materials* (Oxford, Pergamon).
17. Juhas, P., Cherba, D.M., Duxbury, P.M., *et al.*, 2006, Nature **440**, 655.
18. Palosz, B., Grzanka, E., Gierlotka, S., *et al.*, 2002, Z. Kristallogr., **217**, 497.
19. Grzanka, E., Stel'makh, S., Gierlotka, S., 2004, J. Alloys Compd., 382, 133.
20. Wojdyr, M., Mo, Y., Szlufarska, I. (unpublished).
21. Williamson, G.K., Hall, W.H., 1953, Acta Metall. **1**, 22.
22. Balzar, D., 1992, J. Appl. Cryst. **25**, 559.
23. Balzar, D., Audebrand, N., Daymond, *et al.*, 2004, J. Appl. Cryst.. **37**, 911.
24. Scardi, P., Leoni, M., 2006, J. Appl. Cryst. **39**, 24.
25. Chen, D., Sixta, M.E., Zhang, X.F., *et al*., Acta Mater. **48**, 4599.

Acknowledgements. IS kindly acknowledges support from the US NSF grant DMR-0512228, SS and BP acknowledge the support by the Polish Ministry of Education and Science, grant 3T08A 02029.